HAL
open science

Playing with Emulsion Formulation to Control the Perforation of a Freely Expanding Liquid Sheet

Clara Vernay, Laurence Ramos, Alois Würger, Christian Ligoure

To cite this version:

Clara Vernay, Laurence Ramos, Alois Würger, Christian Ligoure. Playing with Emulsion Formulation to Control the Perforation of a Freely Expanding Liquid Sheet. Langmuir, 2017, 33 (14), pp.3458-3467. 10.1021/acs.langmuir.7b00170 . hal-01513239

HAL Id: hal-01513239

https://hal.science/hal-01513239

Submitted on 16 Jan 2018

HAL is a multi-disciplinary open access archive for the deposit and dissemination of scientific research documents, whether they are published or not. The documents may come from teaching and research institutions in France or abroad, or from public or private research centers.

L'archive ouverte pluridisciplinaire **HAL**, est destinée au dépôt et à la diffusion de documents scientifiques de niveau recherche, publiés ou non, émanant des établissements d'enseignement et de recherche français ou étrangers, des laboratoires publics ou privés.

Distributed under a Creative Commons Attribution - NonCommercial - ShareAlike 4.0 International License

Playing with Emulsion Formulation to Control the Perforation of a Freely Expanding Liquid Sheet

Clara Vernay,[†] Laurence Ramos,[†] Alois Würger,[‡] and Christian Ligoure*,[†]

[†]Laboratoire Charles Coulomb, UMR 5521 CNRS, Université de Montpellier, F 34095 CEDEX 05, Montpellier, France

[‡]LOMA, UMR 5798 CNRS, Université de Bordeaux, F 33405 Cedex Talence, France

ABSTRACT: A single drop experiment based on the collision of one drop of liquid on a small solid target is used to produce liquid sheets that are visualized with a fast camera. Upon impact, the drop flattens into a sheet that is bounded by a thicker rim and radially expanding in air. Emulsion based liquid sheets are destabilized through the nucleation of holes that perforate the sheet during its expansion. The holes grow until they merge together and form a web of ligaments, which are then destabilized into drops. We propose the perforation mechanism as a sequence of two necessary steps. The emulsion oil droplets first enter the air/water interface, and then spread at the interface. We show that the formulation of the emulsion is a critical parameter to control the perforation as the addition of salt or amphiphilic copolymers can trigger or completely inhibit the perforation mechanism. We demonstrate that the entering of the droplets at the air/water interface is the limiting step of the mechanism. Thin film forces such as electrostatic or steric repulsion forces stabilize the thin film formed between the interface and the approaching oil droplets, thus preventing the entering of droplets at the interface and in turn inhibiting the perforation process. We theoretically rationalize the successive steps in the approach and entering of an oil droplet at the film interface and the role of salt and amphiphilic polymer in the different steps.

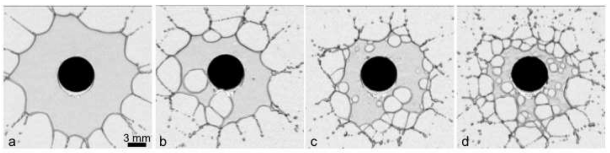

INTRODUCTION

One of the major environmental issues related to the spraying of pesticides on cultivated crops is the drift phenomenon. Because of the wind, small droplets may drift away from the targeted crop and cause contamination. One way to reduce the drift is to decrease the proportion of the smallest drops in the spray (typically, drops with a diameter smaller than 150 μm). In this context, an active area concerns the development of antidrift additive, including dilute oil in water emulsions. When sprayed through a hydraulic nozzle, dilute emulsions have been found to increase the volume median diameter of the drops issued from the spray and decrease the volume fraction of small drops.[1−4] At the exit of the nozzle, a free liquid sheet is formed and subsequently destabilized into ligaments that break into droplets. In a seminal publication, Dombrovski and Fraser[5] observed that liquid sheets produced from dilute emulsions experience a supplementary specific destabilization process which implies perforation events: holes nucleate in the liquid sheet and grow until forming a network of ligaments, which fragments into drops. In a spray, the thickness of the sheet decreases inversely to the distance from the nozzle.[6] The size of the drops resulting from the Rayleigh Plateau destabilization of a ligament scales with the diameter of the ligaments which itself is expected to scale with the thickness of the sheet. Consequently, the drops resulting from the sheet destabiliza tion will be larger as the sheet is thicker, yielding bigger droplets as observed experimentally.[3,4] The physical origin of the perforation events have long remained controversial and two mechanisms were generally invoked: (i) dewetting an oil droplet inclusion by the fluid when its size exceeds the sheet thickness, so that inclusions cause perforation by puncturing both interfaces[5] or (ii) entering and spreading of an oil droplet at the air/water interface inducing a thinning of the film by a Marangoni effect leading ultimately to the film rupture.[7] But these mechanisms had never been confronted to robust experimental results up to recently.[8] To address this question, we have used a milli fluidic experiment based on the collision of one drop of liquid on a small solid target to produce and visualize free liquid sheets using fast video imaging.[9] Upon impact, the drop flattens into a sheet, which is bounded by a thicker rim and radially expands in air, and exhibits destabilization mechanisms similar to those of liquid sheets formed through hydraulic nozzles.[4] A very good quantitative correlation between the cumulated number of perforation events in a liquid sheet of emulsion in the milli fluidic experiment and the proportion of smallest droplets in a real spray of the same emulsion has been obtained, the higher is the number of perforation events, the smaller is the proportion of driftable droplets in the spray. These results suggest that the emulsion droplets are at the origin of the perforation events and that the single drop model experiment is appropriate to investigate and gain understanding of the physical mechanisms governing the perforation mechanism and the spray drop size distribution of antidrift formulations. Thanks to time and space resolved measurements of the thickness field of a dyed sheet, we have found that each perforation event is systemati

cally preceded by the formation of a prehole that thins locally the sheet and widens with time.[8] The growth dynamics of the prehole, whose radius scales with time t as $t^{3/4}$, follows the theoretically predicted law for a liquid spreading on another liquid of higher surface tension due to Marangoni stresses.[10−12] The driving stress due to the surface tension gradient is associated with the presence of an oil droplet at the air/liquid interface. This stress induces the spreading of the oil and results in a viscous shear stress that causes the liquid in the film to flow along the surface tension gradient leading to a localized thinning of the film down to its rupture. Note that the spreading of the oil droplet at the air/water interface requires a positive spreading coefficient S defined as $S = \gamma_{air/aq} - \gamma_{aq/oil} - \gamma_{air/oil}$ where $\gamma_{a/b}$ stands for the interfacial tension between phases "a" and "b", and "aq" stands for the aqueous phase.

Before to spread at the air/water interface, a first necessary step is the entry of the oil droplet from the solvent subphase to the air/water interface. This first step is facilitated by the thinning of the liquid sheet with time due to its expansion. The entry is thermodynamically described by the entering coefficient, E, defined as $E = \gamma_{air/aq} + \gamma_{aq/oil} - \gamma_{air/oil}$. The value of E predicts whether a droplet will enter the interface or remain submerged,[13] $E > 0$ meaning that it is thermodynamically favorable for an oil droplet to enter the air/aqueous phase interface from the aqueous phase (see Figure 1).

Figure 1. Scheme of the physical meaning of the entering coefficient, E. Adapted from ref 14.

A positive entering coefficient is a necessary condition for drop entry, but it is not sufficient. E only indicates if the entering of oil droplets is thermodynamically favorable but does not take into account various surface forces (including electrostatic repulsions, van der Waals attractions and steric forces) that are susceptible to stabilize the thin aqueous film formed between the air/aqueous phase interface and the approaching oil droplet.[15] These thin film forces may stabilize the aqueous film and so kinetically hinder or suppress the drop entering if the lifetime of the liquid sheet is smaller that the typical time to overcome the energy barrier for entry. The aim of this work is to investigate the influence of the formulation of the emulsions in the perforation process of liquids sheets using a milli fluidic model experiment. Formulation is indeed expected to be a critical parameter to control the thin film forces, thus the typical time scale for perforation events, and in fine the antidrift performance of agricultural sprays.

We study emulsions stabilized by ionic (either anionic or cationic) water soluble surfactants. We quantify successively the role of surfactant concentration, addition of electrolyte and addition of amphiphilic copolymer on the two steps of the perforation process: the entering and the spreading of oil droplets at the air/water interface. Finally, we discuss these experimental results in the light of simple theoretical considerations.

MATERIALS AND METHODS

Materials. We study dilute oil in water emulsions. We use methyllaurate, a methyl ester with a alkyl chain composed of 12 carbon atoms, an oil commonly used as antidrift adjuvant for agricultural sprays. In all experiments, the oil content is fixed at 0.3% v/v. The emulsions are stabilized either by an anionic surfactant, sodium dodecyl sulfate (SDS), or a cationic surfactant, cetylpyridinium chloride (CpCl), in Milli Q water. Methyllaurate, SDS, and CpCl were purchased from Sigma Aldrich. Methyllaurate and SDS were used as received, and CpCl was purified in the laboratory by three successive recrystallizations.

For the SDS stabilized emulsions, we used SDS concentration, C_{SDS}, in the range 0.1−2.5 g/L, corresponding to molar concentrations in the range 0.35−8.67 mM. Thus, C_{SDS} is below the critical micelle concentration (CMC), or comparable to the CMC (the CMC of SDS in pure water is 2.4 g/L). Sodium chloride (from Sigma Aldrich) is eventually added to the aqueous phase at a weight concentration C_{NaCl} ranging from 5 to 40 g/L, i.e., molar concentration ranging from 0.09 to 0.68 M.

For the CpCl stabilized emulsions, the surfactant concentration, C_{CpCl}, is fixed at 0.3 g/L (i.e., 0.9 mM) corresponding to the CMC of CpCl in pure water. A monovalent salt (NaCl) or a divalent salt (sodium sulfate, Na_2SO_4, purchased from Merck) is eventually added to the aqueous phase. The NaCl concentration C_{NaCl} ranges between 1 and 20 g/L (i.e., between 0.02 and 0.34 M), and the Na_2SO_4 concentration ranges between 0.07 and 2.84 g/L (i.e., between 0.5 and 20 mM). In addition, a water soluble polymer, Pluronic F108 (from Serva Electrophoresis GmbH), is eventually added to the aqueous phase of the emulsion. F108 (average molecular weight 14000 g/mol) is a triblock copolymer composed of a poly(propylene oxide) (PPO) central chain of approximately 56 monomers flanked at each extremity by a poly(ethylene oxide) (PEO) chain of approximately 132 monomers. The radius of gyration of the PEO blocks is 2.6 nm.[16] At room temperature, the PPO central block of the polymer is hydrophobic and the two PEO lateral blocks hydrophilic. Therefore, F108 macromolecules can adsorb at the hydrophobic/aqueous interface due to its amphiphilic nature. F108 concentration, C_{F108}, ranges from 0.1 to 1% w/w. These concentrations are below CMC (3% w/w at 20 °C[17]), implying that the polymer molecules are fully dissolved and present in the solution as unimers and not micelles. Note that we restrict our experiments with F108 to emulsions stabilized by a cationic surfactant because PEO chains, as most of the water soluble neutral polymers, exhibit attractive interactions with anionic surfactants such as SDS but not with cationic surfactants.[18]

Emulsions are prepared by mechanically stirring using a T18 digital Ultra Turax provided by IKA the oil phase with the aqueous phase that comprises the surfactant (SDS or CpCl), and eventually the salt (NaCl or Na_2SO_4) and/or the F108 polymer. We used a stirring time of 1 min and a rotational velocity of 6,000 rpm. The size distribution of the emulsion drops is measured by laser granulometry using the Mastersizer 2000 from Malvern instrument. For SDS stabilized emulsions without salt, we measure that the mean oil droplet diameter d_{oil} decreases from 20.3 to 9.6 μm as C_{SDS} increases from 0.1 to 2.5 g/L. In addition, we find, for a fixed SDS concentration (C_{SDS} = 2.5 g/L), that the droplet size distribution does not vary with the NaCl concentration: $d_{oil} = 9.4 \pm 1.9$ μm, as averaged over salt concentration 0to 40g/l. Similarly, for CpCl stabilized emulsions, the addition of monovalent or divalent salts and the addition of F108 copolymer do not drastically modify the drop size distribution. We find $d_{oil} = (13.3 \pm 2.0)$ μm (as averaged over the different compositions of the aqueous phase).

Methods. Thin sheets freely expanding in air are produced by impacting a single drop of fluid on a solid target of size comparable to that of the drop. The setup, initially designed by Rozhkov et al.,[19] has been described elsewhere.[9] In brief, we use a hydrophilic cylindrical target of diameter d_t = 6 mm, slightly larger than the drop diameter d_0 = (3.62 ± 0.08) mm. The liquid drop is injected from a syringe pump through a needle placed vertically above the target. The drop falls from a distance 91.0 cm yielding a velocity at impact of $v_0 \approx 4$ m/s. The size of the falling droplets is dictated by the inner diameter of the syringe and the equilibrium surface tension of the samples. In order to maintain a constant droplet size, needles with different diameters are used to account for the various equilibrium surface tension of the samples. After the drop impact, a liquid sheet freely expands in air. The sheet is bounded by a thicker rim that destabilizes into ligaments,

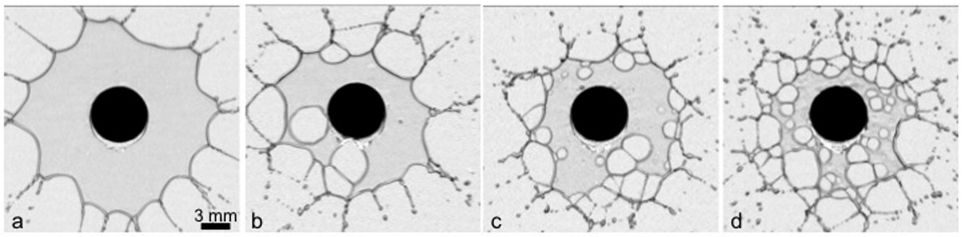

Figure 2. Images of liquid sheets produced with SDS stabilized emulsions (C_{SDS} = 2.5 g/L) and comprising different NaCl concentrations: (a) C_{NaCl} = 0 g/L, (b) C_{NaCl} = 10 g/L, (c) C_{NaCl} = 20 g/L, and (d) C_{NaCl} = 40 g/L. g/L b). All images are taken 3.6 ms after the impact of the drop.

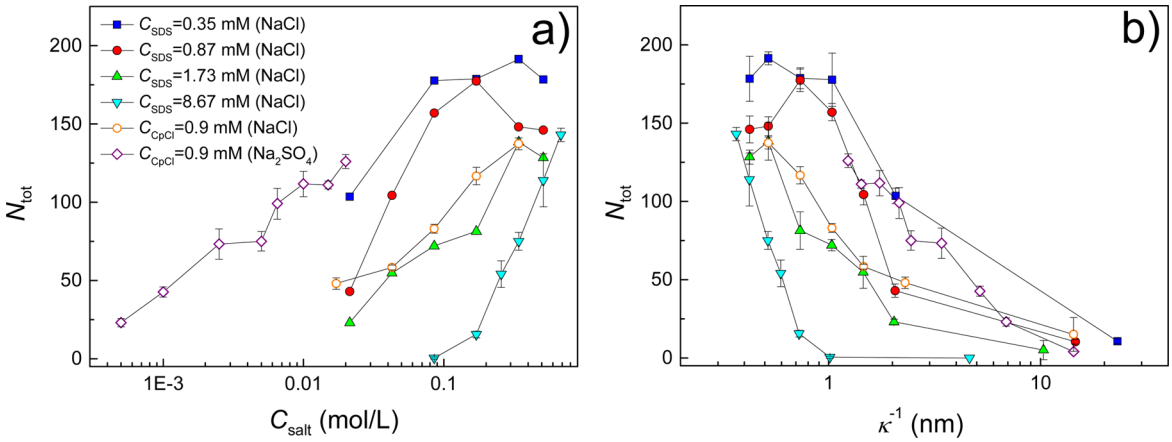

Figure 3. (a) Evolution of the total number of perforation events, N_{tot}, with the salt (NaCl and Na_2SO_4) concentration of the aqueous phase of emulsions stabilized by anionic (SDS) or cationic (CpCl) surfactants. (b) Same data as in (a) but plotted as a function of the Debye length of the aqueous phase κ^{-1}.

which subsequently disintegrate into drops. The sheet then retracts due to surface tension. The sheet reaches its maximum expansion 4 ms after the impact, and its complete lifetime is 10 ms. Time series are recorded after the impact of the drop using a high speed camera Phantom V7.3 (800 pixels × 600 pixels, operated at 9708 frames/s). The perforation of the emulsion based liquid sheet is characterized by the quantification of the total number of perforation events N_{tot} as reported in ref 4, For some experiments, we investigate the localized thinning of the liquid film (prehole) using the method detailed in ref 8: a dye is added to the emulsion aqueous phase (erioglaucine at a concentration of 2.5 g/L) and the thickness field of the sheet loaded with dye is determined thanks to a time and space resolved measurement of the absorbance of the sheet.

To investigate the entry of oil droplets at the air/aqueous phase interface, we monitor the coalescence of oil droplets with the interface. The experimental setup we use has been originally designed by Hotrum et al.[20] The idea is to measure the time evolution of the surface tension of the emulsion aqueous phase with a Wilhelmy plate tensiometer upon injection of a minute volume of emulsion below the interface. The entering and spreading of oil droplets at the air/aqueous phase interface are detected by a sharp decrease of the surface tension due to the presence of an oil film at the surface, allowing one to estimate the time needed for surfactant stabilized oil droplets to enter the interface. A 5 cm diameter Petri dish is filled with 20 mL of the emulsion aqueous phase. A tube connected to a syringe is fixed at the bottom of the Petri dish. Thanks to a syringe pump, a small volume of emulsion (0.15 mL) is injected at approximatively 1 cm below the interface, with a flow rate of 0.12 mL/min. The dead volume of the tube is equal to 0.08 mL, and therefore, only 0.07 mL is effectively injected in the Petri dish.

RESULTS

Role of Electrostatic Interactions on Sheet Perforation. *Cumulated Number of Perforation Events.* We study the destabilization of liquid sheets made of emulsion stabilized either by an anionic (SDS) or a cationic (CpCl) surfactant. The concentrations of surfactant in the aqueous phase are roughly equal to the CMC (C_{SDS} = 8.67 mM and C_{CpCl} = 0.9 mM). Figure 2 shows images of the sheets for different concentrations of NaCl (C_{NaCl} = 0, 10, 20, 40 g/L) in the emulsion aqueous phase taken at the same time after the drop impact for SDS stabilized emulsions. Without salt (Figure 2a), the liquid sheet is destabilized by the ejection of drops from the rim, a mechanism similar to that of a pure water liquid sheet. No perforation of the sheet is detected in this case. Interestingly, we find however that the addition of salt triggers the perforation of the liquid film (Figure 2b−d). Qualitatively, the images suggest that the numbers of holes increases as C_{NaCl} increases. The same effect is observed for CpCl stabilized emulsions (photos not shown).

To quantify the perforation instability, we plot in Figure 3 the cumulated number of perforation events, N_{tot}, that occur during the full life of the sheet, as a function of the salt concentration (Figure 3a) or as a function of the Debye length, κ^{-1}, the characteristic length scale for the electrostatic interaction (Figure 3b), where

$$\kappa^2 = 4\pi l_B(q_+{}^2 n_+ + q_-{}^2 n_-) \quad (1)$$

with the ion valencies $q_\pm$, molar concentrations $n_\pm$, and Bjerrum length l_B = 0.7 nm. For all surfactant concentrations, we observe that N_{tot} increases with the salt concentration, decreases with κ^{-1}, eventually reaches a plateau at higher salt concentration, lower Debye length. The less is the surfactant concentration, the more rapidly the plateau is reached, and the highest is the plateau value. For a given Debye length, the total number of perforation events spans over 1 order of magnitude

depending on the surfactant concentration. At the same molar concentration, the divalent salt (Na_2SO_4) is much more efficient than the monovalent salt (NaCl) to promote the perforation as observed for a fixed CpCl concentration, due to a smaller Debye length for a divalent salt. Overall, the data show that the perforation process is limited or even completely inhibited when the range of the electrostatic repulsion forces increases sufficiently.

To rationalize these results, we separately investigate the influence of the salt and surfactant concentrations on the two steps of the perforation mechanism: first the entry of the oil droplets at the air/water interface and second their spreading.

Spreading Dynamics. We use the method detailed in ref 4 and briefly described in the Materials and Methods section to quantify the opening dynamics of the local thinning of the sheet, hereafter called a prehole, due to the spreading of an oil droplet at the air/water interface. The data acquired with all aqueous phases investigated collapsed on a single curve (Figure 4). Moreover, we find that, the radius of the prehole R_{ph}

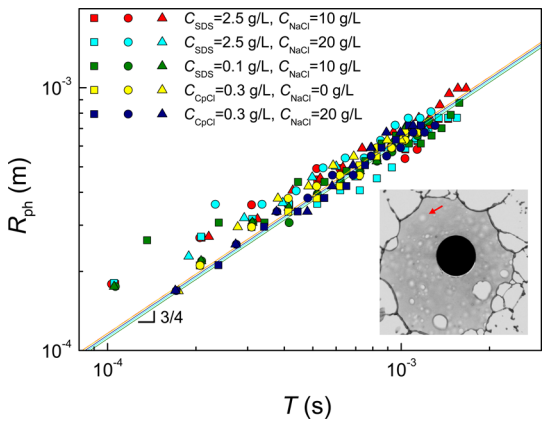

Figure 4. Evolution of the radius of the prehole, R_{ph}, with T, the time elapsed since the prehole formation for emulsions with various formulations as indicated in the legend. Symbols are data points (different symbols correspond to different experiments) and lines are power law fits with an exponent 3/4. Inset: Image of a liquid sheet produced with dyed (with erioglaucine) emulsion (C_{SDS} = 0.1 g/L and C_{NaCl} = 10 g/L) that allows one to visualize the local thinning of the sheet due to the entering of oil droplet at the air/solution interface. The target (black disk) of diameter 6 mm sets the scale. The red arrow points to one prehole.

increases with T, the time elapsed since its formation, as a power law with an exponent 3/4 (Figure 4). This result is in full agreement with our previous measurements for emulsion stabilized by non ionic surfactants[8] and so confirm a widening dynamics driven by a Marangoni spreading[10−12] for which it has been theoretically predicted $R_{ph} = kT^{3/4}$, with $k = \sqrt{\frac{4}{3}}\frac{S^{1/2}}{(\rho\eta)^{1/4}}$, where S is the spreading parameter, η is the zero shear viscosity, and ρ is the density of the aqueous phase. Here, the excellent collapse of all curves of the prehole radius evolution, whatever the salt and surfactant concentrations, unambiguously demonstrate that the nature and concentration of the surfactant and the salt concentration do not modify the widening dynamics of preholes and so the spreading of oil droplets at the air/water interface.

Entering of Oil Droplets at the Air/Aqueous Phase Interface. We investigate the influence of the salt and surfactant concentration on the entering of oil droplets at the air/aqueous phase interface that we have identified as the first step of the perforation mechanism. To do so, we monitor the evolution of the surface tension measured at the air/aqueous phase interface during the entering of emulsion oil droplets. Three SDS stabilized emulsions comprised a fixed surfactant concentration (C_{SDS} = 2.5 g/L) and variable salt concentrations (C_{NaCl} = 0, 10, 20 g/L) NaCl are investigated. The black arrows in the plot of the time evolutions of the surface tension (Figure 5) mark the

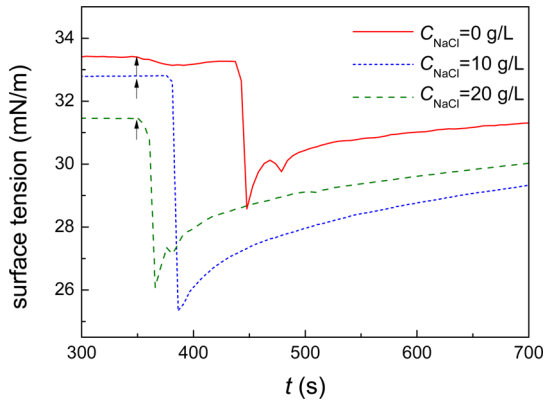

Figure 5. Time evolution of the surface tension of an aqueous phase upon injection below the air/aqueous phase interface of oil droplets dispersed in the same aqueous phase. The aqueous phases contains SDS at a concentration C_{SDS} = 2.5 g/L and different NaCl concentrations as indicated in the legend. The black arrows indicate the time of injection.

injection time of the emulsion. For each sample, before the injection of the emulsion, a plateau corresponding to the equilibrium surface tension of the emulsion aqueous phase is measured. After the injection, a sharp decrease of the surface tension corresponding to the entering and spreading of oil droplets at the interface is systematically measured but the time elapsed from the injection to the drop of the surface tension (considered as the entering time) strongly depends on the salt concentration in the aqueous phase. We measured that this time decreases from 81 ± 18 s without NaCl, to 36 ± 7 s for C_{NaCl} = 10 g/L and to 27 ± 7 s for C_{NaCl} = 20 g/L. Here the errors bars correspond to standard deviations calculated over four repetitions of the same experiments. It is instructive to compare this time to the time expected from the simple creaming of oil droplets at the interface. The creaming velocity reads

$$v_{\text{creaming}} = \frac{1}{18}\frac{\Delta\rho g d_{\text{oil}}^{2}}{\eta} \tag{2}$$

with $\Delta\rho$ being the density difference between the aqueous and oil phases of the emulsion, η being the viscosity of the aqueous phase, and d_{oil} being the diameter of the oil droplets. For a droplet with d_{oil} = 20 μm, setting at 1 cm from the interface (distance from the tip of the tube to the air/water interface) the time to reach the interface is around 330 s. This time is much longer than the entering time measured experimentally. This is presumably due to the fact that the oil droplets have an initial velocity when their are injected in the solution, and thus reach more rapidly the interface.

Note that this experimental setup does not exactly mimic the entering of oil droplet at the air/aqueous phase interface during the sheet expansion. Indeed, the surface tensions measured correspond to equilibrium surface tensions as the oil enters a

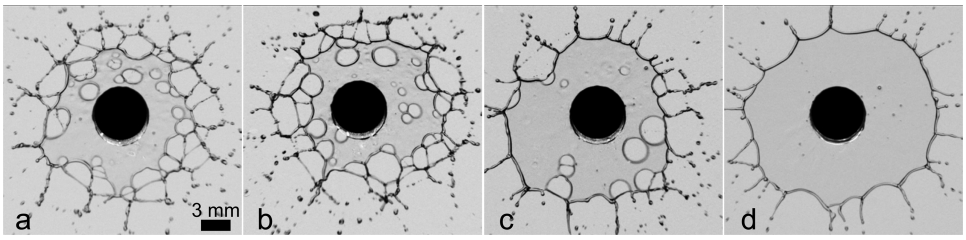

Figure 6. Images of liquid sheets made of emulsions stabilized by CpCl. The aqueous phase contains a fixed NaCl concentration (20 g/L) and various Pluronic F108 concentrations, C_{F108} = 0 g/L (a), 2.5 g/L (b), 4 g/L (c), and 7.5 (d) g/L. Images are taken 3.6 ms after the impact of the drop.

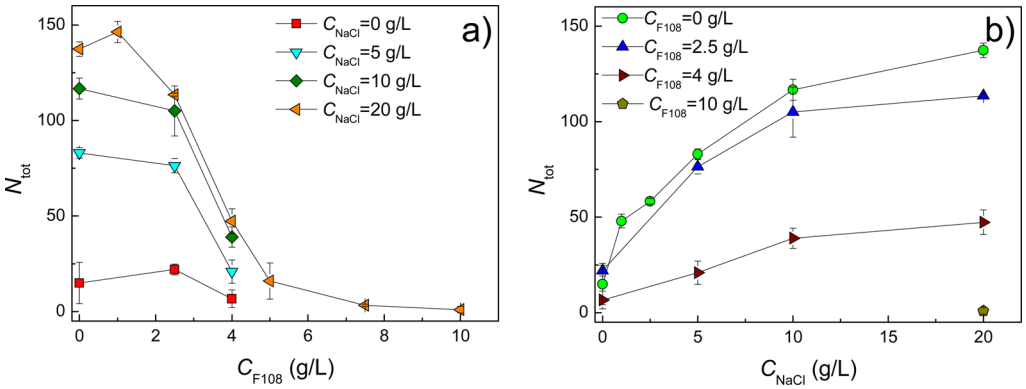

Figure 7. Evolution of the total number of perforation events, N_{tot}, with (a) the Pluronic F108 concentration, for different NaCl concentrations as indicated in the legend, (b) the NaCl concentration, for different F108 concentrations as indicated in the legend. All emulsions are stabilized by CpCl.

still air/water interface, whereas the interface is in expansion during the single drop experiment. We nevertheless firmly believe that the setup provides quantitative information on the tendency of oil droplets to enter the air/aqueous phase interface. We can reasonably think that the entry must be facilitated by the expansion of the interface (as it will entail a decrease of surfactant concentration at the interface) and so the entering times in the single drop experiment are expected to be shorter than the ones measured with the present setup.

In conclusion, these experimental results highlight that the addition of salt in the aqueous phase of emulsions stabilized by ionic surfactants promotes the entering of emulsion oil droplets at the air/aqueous phase interface.

Effect of Steric Interactions on Sheet Perforation. Amphiphilic copolymer chains are expected to adsorb at the interfaces thus creating steric repulsion between the oil droplets and the air/aqueous phase interface. The objective is here to investigate the possible role of those steric repulsions to the perforation processes.

Cumulated Number of Perforation Events. Amphiphilic triblocks copolymer (Pluronic F108) is added to the aqueous phase of the emulsion. We investigate the influence of F108 concentration on the sheet perforation for different sodium chloride concentrations (C_{NaCl} = 0, 10, 20 g/L). Figure 6 shows images of the sheets for different concentrations of F108 in the aqueous phase of the emulsion taken at the same time after the drop impact, for C_{NaCl} = 20 g/L. As observed previously, without F108 and at high salt concentration (C_{NaCl} = 20 g/L), a large number of perforation events are observed in the liquid sheet (Figure 6a). The addition of F108 entails a continuous decrease of N_{tot} (Figure 6b,c), and for C_{F108} = 7.5 g/L we do not observe any perforation of the liquid film (Figure 6d).

We plot in Figure 7a the evolution of the total number of perforation events, N_{tot}, with the F108 concentration in the emulsion aqueous phase for different NaCl concentrations. For a given salt concentration, we find that the increase of C_{F108} leads to a large decrease of N_{tot}. For C_{NaCl} = 20 g/L, N_{tot} decreases from 146 for C_{F108} = 1 g/L down to 3 for C_{F108} = 7.5 g/L. Hence, the addition of F108 permits to completely inhibit the perforation process. The same phenomenon is observed for different salt concentrations, but we find that a decrease of C_{NaCl} entails a shift of the curve toward smaller values of N_{tot}. The influence of the salt concentration on the sheet perforation is highlighted in Figure 7b, where the same data as in Figure 7a are plotted as a function of C_{NaCl} for various C_{F108}, from 0 to 10 g/L. This representation emphasizes that an increase of the salt concentration leads to an increase of the total number of perforation events and that this effect is stronger as the Pluronic F108 concentration is lower.

Spreading Dynamics. We investigate the effect of addition of amphiphilic copolymer to the spreading dynamics of oil droplets at the air interface of the expanding liquid sheet. Measurements are performed for two different compositions of the aqueous phase with equal salt concentration (C_{NaCl} = 20 g/L) but different F108 concentrations (C_{F108} = 0, 5 g/L). Consistently with data obtained without dye, many perforation events occur when the amount of polymer is low ($N_{tot} \approx 137$), while few perforation events occur at higher F108 concentration ($N_{tot} \approx 16$). Figure 8 displays the evolution of the prehole radius, R_{ph}, as a function of the time elapsed since its formation, T, for the two compositions of the aqueous phase. We find a collapse of the different sets of data. Furthermore, in all cases, $R_{ph} = kT^{3/4}$, in agreement with our results described above obtained with various salt concentrations and with previous results obtained for non ionic emulsions.[8] This

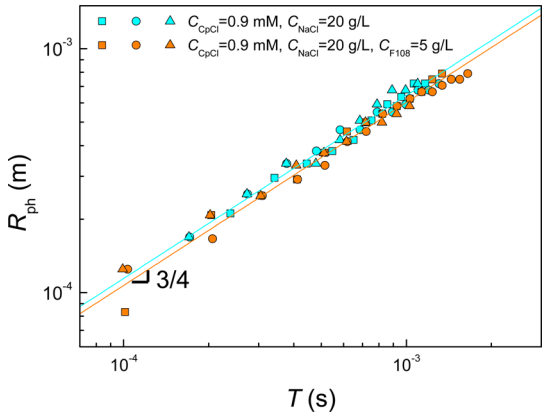

Figure 8. Evolution of the radius of the prehole, R_{ph}, with T being the time elapsed since the prehole formation for emulsions with various formulations as indicated in the legend. Symbols are data points (different symbols correspond to different experiments), and lines are power law fits with an exponent of 3/4.

confirms a widening dynamics of prehole independent of the presence of amphiphilic copolymer and in agreement with the dynamics of Marangoni spreading.

Entering of Oil Droplets at the Air/Aqueous Phase Interface. We assess the entering properties of emulsion oil droplets at the air/aqueous phase interface and show (Figure 9)

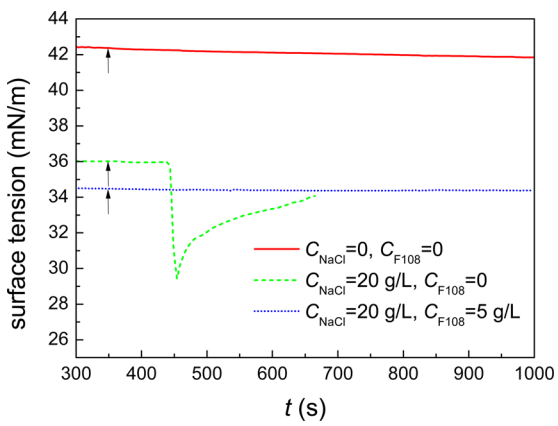

Figure 9. Time evolution of the surface tension of an aqueous phase upon injection below the air/aqueous phase interface of oil droplets dispersed in the same aqueous phase. The aqueous phases contains CpCl (C_{CpCl} = 0.9 mM) and eventually salt and Pluronics F108, as indicated in the legend. The black arrows indicate the time of injection.

the time evolution of the surface tension measured at the air/aqueous phase interface during the entry of oil droplets, for three compositions for the aqueous phase (comprising either only surfactant, or surfactant and salt, or surfactant, salt, and amphiphilic polymer, see exact composition in the figure legend). The overall behavior of the curves is similar to that of Figure 5. Consistently with the experiments with anionic surfactant, addition of salt facilitates the entry of oil droplets at the interface as revealed by a decrease of the characteristic time for drop of the surface tension. This effect is even stronger than that observed with SDS as surfactant, since, without salt, no decrease is measured during the whole experiment (1000 s, i.e., 650 s after the injection of emulsion below the interface). Interestingly, the presence of F108 in addition to salt also prevents the entry of oil droplet as no drop of surface tension is measured during the whole duration of the experiment.

In conclusion, the addition of salt in the aqueous phase of CpCl stabilized emulsions promotes the entry of oil droplets at the air/aqueous phase interface. On the contrary, the addition of an amphiphilic copolymer in the aqueous phase of emulsion stabilized by CpCl and NaCl hinders the entry.

DISCUSSION

We have shown that we can vary the formulation of the emulsion to tune the electrostatic and/or steric barriers for the entry of an oil emulsion at the water/air interface, whereas the formulation does not play any role in the spreading dynamics of the oil droplet once at the interface. The existence of an energetic barrier slows down the entry step. If the characteristic time for this step exceeds the lifetime of the liquid sheet, entry in the air/water interface and perforation of the sheet will not occur. Beside the short range repulsive forces, hydrodynamic forces and fluctuation forces are also expected to contribute to the entry mechanism. The aim of this section is to rationalize the successive steps (and their durations) for the approach and entry of an oil droplet at the film interface.

Here we discuss how a charged spherical droplet is advected toward and enters at the interface of a thinning liquid film. Because of the high surface viscosity of the surfactant monolayer that covers the droplet, the interface does not flow and the droplet may be considered as a solid particle of radius a with no internal flow. We define D as the minimal distance from the surface of the droplet to the air/water interface. In a first step we determine the time at which the droplet reaches the interface (advection), and then discuss how the droplet enters the interface (coalescence).

Advection. We study how a floating droplet approaches the film surface. The stagnation flow in a thinning film advects the droplet toward the interface. The thickness of the mature incompressible film decreases with the radial distance from the center of the sheet and time according to $h(r, t) \propto \frac{1}{rt}$. and the velocity field within the moving film reads $u_r(r, t) = \frac{r}{t}$ in the radial direction[9,21] and $u_z(z, t) = -2\frac{z}{t}$ in the vertical direction (incompressibility condition). In the following, the lower (respectively upper) interface of the film correspond to $z = 0$ (respectively $z = h$).

Free Advection Regime (D > a). If the distance D exceeds the radius of the droplet, its presence does not disturb the velocity field due to film thinning. Then the droplet is advected toward the film surface with the velocity $\dot{D} = u_z(D, t) = -2\frac{D+a}{t}$, is directly given by the thinning rate of the film. Free advection ends as the droplet reaches $D = a$, and occurs at a time t_a which is given by

$$\frac{t_a}{t_0} = \left(\frac{D_0 + a}{2a}\right)^{1/2} \tag{3}$$

Here, t_0 is an initial time, that we take as the impact time of the drop, defined as the ratio between the diameter of the drop (~3.6 mm) and its velocity at impact (~4 m/s), $t_0 \approx 1$ ms. Since the initial distance D_0 is comparable to, or smaller than, the initial sheet thickness $h_{max} \lesssim 250$ μm, the time $t_a - t_0$ is of the order of the experimental time of maximal sheet expansion.

Lubrication Regime ($a > D > D_*$). In the lubrication regime, when the sphere is close to the liquid interface, $D < a$, the

droplet slows down due to the hydrodynamic coupling to the interface. In that case, a good approximation for the force exerted by the unperturbed ambiant flow u_z is provided by the solution for the near contact limit: $D \to 0$.[22] The droplet velocity is determined by equilibrating the force due to the advection flow and the friction force, $F_{adv} + F_S = 0$. The former is similar to the force in the free advection regime, $F_{adv} = 6\pi f\eta a u_z$, albeit with an additional numerical factor $f = 2.039$. On the other hand, the friction force for small D is known from lubrication theory at fluid interfaces:[23] $F_S = -\frac{6\pi\eta a^2}{4}\frac{\dot{D}}{D}$.

Equilibrating these forces, we find the particle velocity $\frac{\dot{D}}{D} = -\frac{8f}{t}$ (here $z = a + D \simeq a$), which upon integration with the initial conditions $D(t_a) = a$, leads to $D(t) = a\left(\frac{t_a}{t}\right)^{8f}$. This regime ceases to be valid as soon as the distance D_* is of the order of the Debye length (respectively, the thickness of the polymer layer) for an electrostatic (respectively, steric) barrier. For shorter distances, the electric double layer (respectively, polymeric layer) exerts an additional, much larger, force which prevents the drop from further approaching the interface. The time t_* at which electrostatic forces (and/or steric forces) set in reads

$$t_* = t_a\left(\frac{a}{D_*}\right)^{1/8f} \tag{4}$$

With $8f \approx 16$, one finds that the lubrication regime is of minor importance. Indeed, because D_* is of the nanometer range, $a \gg D_*$, t_* is only slightly larger than t_a, and the duration of the lubrication regime $t_* - t_a$ is negligible.

Note that eq 4 has been calculated assuming a free air−water interface. If the water film is covered with surfactants, a no slip boundary condition would be more appropriate, and the factor $8f$ should be replaced with $2f'$ where $f' \approx 1$, changing significantly the duration of advection. We can estimate the time needed for a SDS molecule to diffuse at the interface by a diffusion limited process. The time evolution of the surfactant surface concentration, Γ, is given by $\Gamma = 2\sqrt{\frac{D_b t}{\pi}}C_b$ with D_b being the bulk diffusion coefficient of the surfactant and C_b being the bulk surfactant concentration.[24] The diffusion time, t_D, necessary to reach the equilibrium surfactant surface concentration, Γ_{eq}, thus reads $t_D = \frac{\pi}{4}\frac{1}{D_b}\left(\frac{\Gamma_{eq}}{C_b}\right)^2$. For SDS, with[25] $D_b = 1.76 \times 10^{-6}\,\mathrm{cm^2/s}$ and[26] $\Gamma_{eq} \approx 3 \times 10^{-10}\,\mathrm{mol/m^2}$ as measured for a surfactant concentration ($C_b = 2.9\,\mathrm{g/L} \simeq 10^{-2}$ mol/L) comparable to that of used in the single drop experiments, one estimates $t_D = 0.4$ ms. Hence, the SDS molecules diffuse at the air/aqueous phase interface in a relatively short time (<1 ms). If the air/water interface is not devoid of surfactant molecules, the duration of the lubrication regime $t_* - t_a$ is imuch larger than the prediction by eq 4. In that case, with $a/D_* \approx 10^3$, one finds $t_*/t_a > 10$, indicating that $t_* - t_a$ would determine the advection time. One would find an advection time much larger than the lifetime of the sheet, inconsistent with our experimental observation. However, one expects that the rapid radial velocity advects any contamination by surfactants and thus cleans the interface. It is therefore reasonable to assume a free air−water interface yielding a negligible duration of the lubrication regime.

Disjoining Pressure. As the droplet gets close to the interface, it becomes immobile at a distance D_* where the hydrodynamic drag is canceled by short range repulsive forces. Here we provide evaluation of the distance D_* and discuss the disjoining pressure due to ionic surfactants and/or nonionic polymers adsorbed on the droplet.

Electrostatics. The droplet is covered by a surfactant monolayer. The mobile counterions released by the charged surfactant are confined within a screening layer of thickness the Debye length κ^{-1}, which decreases with increasing salt content according to eq 1. In Derjaguin approximation, the distance from the surface of the droplet to the air/water interface reads $D_\rho = D_* + \rho^2/2a$, with the radial coordinate ρ defined as the distance from the center of the droplet. The interface squeezes the counterion cloud and thus exerts an electrostatic disjoining pressure; at low or moderate surface charge densities σ, one finds in the Debye−Hückel approximation: $\Pi_{el} = \frac{\sigma^2}{2\epsilon}e^{-D_\rho\kappa} = \Pi_0 e^{-D_\rho\kappa}$. Integrating over the surface, one obtains the electrostatic force[27]

$$F_{el} = 2\pi a\kappa^{-1}\Pi_0 e^{-D\kappa} \tag{5}$$

The droplet becomes immobile at a distance D_* where hydrodynamic and electrostatic forces cancel each other, $F_{el} + F_{adv} = 0$. With the above advection force, we find

$$D_* = \kappa^{-1}\ln\frac{\Pi_0}{3f\kappa\eta u_z} \tag{6}$$

We first provide an evaluation of $\Pi_0 = \frac{\sigma^2}{2\epsilon}$. The maximum coverage of a droplet corresponds to an area per molecule of typically 0.5 nm^2 and, assuming a complete dissociation of the surfactant, to a surface charge density of $\sigma \approx 2e\,\mathrm{nm}^{-2}$. Hence, $\Pi_0 \sim 100$ MPa. In our experimental conditions, κ^{-1} varies between 0.4 and 25 nm (see Figure 3b). With $u_z \sim$ cm/s, we find that D_* decreases from 200 nm at low salt concentration down to 2 nm at high salt concentration. Since both the width and height of the electrostatic barrier $V_{el} = 2\pi a\kappa^{-2}\Pi_0$ increase with the screening length κ^{-1}, this estimate already suggests that charged droplets do not coalesce in a weak electrolyte; upon adding salt, the barrier diminishes and may be overcome by fluctuations.

Grafted Polymer. Adsorption of neutral polymers provides a steric repulsion. The resulting disjoining pressure depends on the grafting density Γ and the radius of gyration of the polymer R_g. At low density ($\Gamma < R_g^{-2}$) and short distances ($D < R_g$), the disjoining pressure reads[28]

$$\Pi_{pol} = k_B T\Gamma\frac{(2\pi R_g)^2}{D^3} \tag{7}$$

In the Derjaguin approximation, the repulsive force thus reads: $F_{pol}(D) = k_B T\Gamma\frac{(2\pi R_g)^2 2\pi a}{D^2}$. The stationary distance, determined by writing $F_{pol} + F_{adv} = 0$, is

$$D_* = \sqrt{\frac{k_B T}{3f\eta u_z}\Gamma(2\pi R_g)^2} \tag{8}$$

With Γ, $R_g^2 \sim 1$, that corresponds to the maximum surface coverage of the low density regime, we find that D_* is of the order of 25 nm.

Dispersion Forces. The disjoining pressure for the water film reads $\Pi_{vdW} = -\frac{H}{6\pi D^3}$, where the Hamaker constant, H, for the

oil−water−air system is usually negative, resulting in a repulsive force. For octane as oil, $H = -0.2 \times 10^{-20}$ J.[27] Thus, even at distances of a few nanometers, $\Pi_{vdW} \approx 20$ Pa is significantly smaller than the estimates for the electrostatic pressure ($\Pi_0 \approx (10^4 - 10^6)$ Pa) and the steric pressure due to the grafted polymers ($\Pi_{pol} \approx 10^6$ Pa). Furthermore, experiments with non ionic surfactants[4] show that the droplets enter the interface rather rapidly (on the time scale of ms), strongly suggesting that dispersion forces are of little significance, and that the hindering barrier is essentially due to the surface charges or adsorbed polymers. Thus, we discard Π_{vdW} in the following discussion.

Interface fluctuations. In the above mean field description the droplet is stabilized at a distance D_* from the film surface. The electrostatic (or steric) forces result in energy barrier. For a Debye length $\kappa^{-1} = 0.4$ nm), (respectively $\kappa^{-1} = 25$ nm, one gets $D_* = 2$ nm (respectively $D_* = 200$ nm) and $V_{el} \approx 20 k_B T$ (respectively $V_{el} \approx 10^6 k_B T$). Those barriers are usually very large compared to $k_B T$ and cannot thus be overcome by the Brownian motion of the droplet.

Thus, we consider fluctuations with respect to the above mean field treatment, concerning the surfactant concentration or the interface profile. Fluctuations of the surface charge density or the polymer grafting density, would locally reduce the energy barrier, yet are prohibited by the corresponding increase in surface energy due to the removing of the surfactants (or polymers) from the contact area. A more favorable situation occurs for local fluctuations ξ of the interface profile; as a simple ansatz we use the Gaussian profile $\xi = D_* e^{-\rho^2/R^2}$ with the lateral length scale R. Its energy consists of electrostatic and capillary contributions. In small gradient approximation, $\nabla\xi \sim D_*/R \leq 1$, the capillary energy $(\gamma/2)\int dS(\nabla\xi)^2$ is independent of R,

$$E_{cap} = \frac{\pi}{2}\gamma {D_*}^2 \tag{9}$$

From the electrostatic disjoining pressure we readily obtain the energy per unit area, $\kappa^{-1}(e^{\kappa(\xi - D_*)} - e^{-\kappa D_*})\,\Pi_0$. Close to the point of contact we have $\xi \approx D_*(1-\rho^2/R^2)$ and find upon integration $E_{el} = \pi\Pi_0\kappa^{-2}R^2/D_*$. Its variation with the later length scale favors $R \approx D_*$, leading to

$$E_{el} = \pi\kappa^{-2}D_*\Pi_0 = \pi\kappa^{-2}D_*\sigma^2/2\epsilon \tag{10}$$

An expression similar to eq 10 can be obtained for grafted polymers. From eq 7, we find a rough estimate for the energy required for compressing the polymer brush to a distance D_{min},

$$E_{pol} = 2\pi k_B T \Gamma (2\pi R_g)^2 \frac{D_*}{D_{min}} \tag{11}$$

Depending on the grafting density, the barrier varies from a fraction of the thermal energy to tens of $k_B T$, and thus may significantly slow down perforation of the water film.

The rate of rupture, assimilated as the rate for the droplet entering the surface, is given by

$$\frac{1}{\tau} = \frac{1}{\tau_0} e^{-(E_{el/pol} + E_{cap})/k_B T} \tag{12}$$

where the attempt frequency $1/\tau_0$ subsumes different mechanisms that contribute to delay the entering of the droplet: For example, the hydrodynamic time scale $\tau_h = aD_*/\nu$ arises from outward flow of water that accompanies the surface fluctuation; with the kinematic viscosity ν of water, $\tau_h \sim 10^{-8}$ s. On the other hand, this outward flow advects the screening ions and thus requires back diffusion which occurs at a time scale $\tau_{ion} = a\kappa^{-1}/D_{ion} \sim 10^{-5}$ s. Finally, ${\tau_0}^{-1}$ accounts for the fact that the fluctuation may occur at any point of the lubrication area $S_{lub} = \pi a D_*$ which, in a similar context, gives rise to a logarithmic factor in the mean square amplitude of interface fluctuations.[29]

The above approach relies on a macroscopic description of the interface and neglects effects on the molecular scale that become important as the droplet approaches the film surface within nanometers. Thus, the surface tension is reduced as the film thickness is of the order of a nanometer. The electrostatic properties change due to the discrete nature of both surface charge and screening cloud; the increase of the single ion self energy in a nanofilm is expected to reduce the degree of dissociation of ionic surfactants. The final phase of the rupture process requires molecular rearrangements of the surfactant water film, which are not captured by the model.

Entering. So far we have discussed the time t_* a droplet takes to travel from its initial position to the air−water interface. With the rate of rupture $1/\tau$ given above, the integrated probability of perforation at time t reads $\phi(t - t_*) = 1 - e^{-(t-t_*)/\tau}$. With the rate $\dot{n}(t_*)$ of droplets arriving at the interface, the total number of perforation events at time t is given by the convolution of $\dot{n}$ and ϕ,

$$N(t) = \int_0^t \phi(t - t_*)\,\dot{n}(t_*)dt_* \tag{13}$$

The rate $\dot{n}$ depends on the radial profile $h(r, t)$ of the film and of its rate of thinning. From our experiments at different surfactant and salt contents it is clear that most droplets reach rapidly the distance D_* and that the perforation events beyond about two milliseconds are delayed to the small rate $1/\tau$. In other words, the time dependence of the number of perforation events N is determined by the probability of rupture ϕ, and in a rough approximation we may assume $N(t) = N_0\phi(t)$.

Figure 10 shows ϕ at some fixed time $t = 3\tau_0$ as a function of the screening length κ^{-1} for three values of the surface charge density σ. Since the electrostatic barrier E_{el} increases with both κ^{-1} and σ, the probability of coalescence strongly decreases for large Debye length and large surface charge. The behavior of Figure 10 compares favorably with the data shown in Figure 3b, thus highlighting the importance of electrostatic repulsion for the stability of the film. This explains also the variation of the

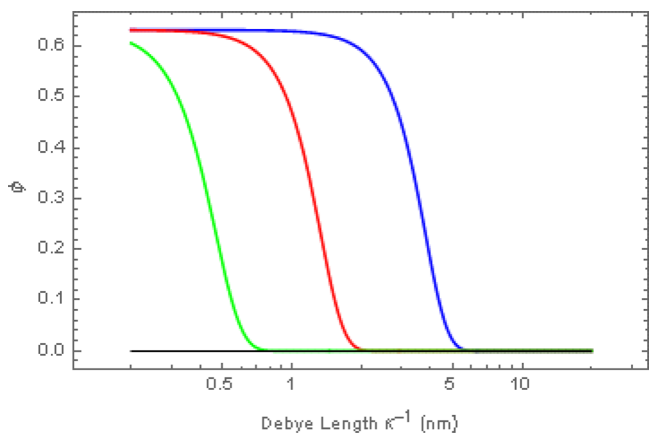

Figure 10. Number of perforation events for three different surface charge densities (from left to right: $\sigma = 0.1e$, $0.03e$, $0.01e$ nm^{-2}), as a function of the screening length κ^{-1}.

number of perforation events with the valency $q_{\pm}$ of the salt ions. Indeed, the dependence of the screening parameter (eq 1) on $q_{\pm}$ provides an almost quantitative description for the difference observed for monovalent and divalent ions.

Yet one should be aware that the above model does not describe the microscopic details of the entering process, but rather subsumes its final step in the constant τ_0 which could be regarded as a fit parameter. In addition, the surfactant accumulating at the film surface could change the hydro dynamic boundary conditions in the lubrication regime during the lifetime of the water sheet, which would result in a wide distribution of the time t_* in eq 13.

CONCLUSION

Nucleation of holes in emulsion based liquid sheets is due to the entry and spreading of oil droplets at the air/aqueous phase interface. Note that the two step mechanism that we have proposed for the perforation presents strong analogies with antifoam action of dilute oil in water emulsions.[30] The two experimental configurations are comparable, both implying the rupture of a liquid film due to the presence of oil droplets dispersed in an aqueous phase. The main differences between the two type of configurations are the range of the film thickness that is typically 10 times larger for liquid sheets than for foam films, and the fast thinning dynamics of the liquid sheet.

In our experiments, the two steps of the perforation mechanism are thermodynamically favorable as the entering and spreading coefficients are both positive for all the investigated systems. By modifying the physical parameters of the emulsions, we have shown that the formulation of the emulsion is a critical parameter to control the perforation. The addition of salt or amphiphilic copolymer in the aqueous phase of emulsions stabilized by water soluble ionic surfactants can kinetically trigger or completely inhibit the perforation mechanism. We have demonstrated experimentally that the entering of the oil droplets at the air/aqueous phase interface is the limiting step for the perforation mechanism. A high entering energy barrier can prevent the droplet entry process. Thin film forces, in particular electrostatic and steric repulsive forces, stabilize the thin aqueous film formed between the air/aqueous phase interface and the approaching oil droplet, thus preventing the entering of droplets. In this case, even if the entering is thermodynamically favorable, the entering process is strongly limited and even suppressed by the enhanced stability of the thin film.

We have identified theoretically successive regimes for the approach of an emulsion droplet to the air liquid interface with three typical durations: (i) a free advection regime during which the droplet, thanks to the thinning down of the expanding sheet, approaches rapidly air/liquid interface down to a distance comparable to the size of the droplet; (ii) a lubrication regime that takes place until the droplet reaches a distance comparable to the characteristic length of the energetic barrier and for which the nature of the air/liquid interface has a strong effect on the hydrodynamic force acting on the droplet; and (iii) an immobilization regime dictated by any strong short range repulsive. This third regime will cease thanks to stochastic local fluctuations of the interface profile leading to the entering of the droplet in the liquid interface. The regime with the longest duration is the limiting step for the perforation process. If its characteristic time is long compared to the lifetime of the liquid sheet, perforation events are significantly reduced or even suppressed.

However, we mention that even if the spreading of oil droplets at the interface is not the limiting step for the perforation, it is nevertheless crucial as several studies have emphasized that solid particles that enter the air/aqueous phase interface but do not spread at the interface do not lead to the perforation of liquid sheets.[2,31]

Overall, our work has allowed one to establish the physical mechanisms at the origin of the antidrift properties of dilute oil in water emulsions and in turn propose new routes to develop novel and more efficient formulations for antidrift emulsion adjuvants.

AUTHOR INFORMATION

Corresponding Author

*E mail: christian.ligoure@umontpellier.fr

ORCID

Christian Ligoure: 0000 0003 3445 6826

Notes

The authors declare no competing financial interest.

ACKNOWLEDGMENTS

The authors thank Jean Christophe Castaing and Antonio Stocco for stimulating discussions. Partial financial support of Solvay is acknowledged.

REFERENCES

(1) Ellis, M. C. B.; Tuck, C. R.; Miller, P. C. H. Dilute emulsions and their effect on the breakup of the liquid sheet produced by flat fan spray nozzles. *Atomization Sprays* **1999**, *9*, 385−397.

(2) Qin, K.; Tank, H.; Wilson, S. A.; Downer, B.; Liu, L. Controlling droplet size distribution using oil emulsions in agricultural sprays. *Atomization Sprays* **2010**, *20*, 227−239.

(3) Hilz, E.; Vermeer, A. W. P. Spray drift review: The extent to which a formulation can contribute to spray drift reduction. *Crop Prot.* **2013**, *44*, 75−83.

(4) Vernay, C.; Ramos, L.; Douzals, J. P.; Goyal, R.; Castaing, J. C.; Ligoure, C. Drop impact experiment as a model experiment to investigate the role of oil in water emulsions in controlling the drop size distribution of an agricultural spray. *Atomization Sprays* **2016**, *26*, 827−851.

(5) Dombrowski, N.; Fraser, R. P. A Photographic Investigation into the Disintegration of Liquid Sheets. *Philos. Trans. R. Soc., A* **1954**, *247*, 101−130.

(6) Dombrowski, N.; Hasson, D.; Ward, D. E. Some aspects of liquid flow through fan spray nozzles. *Chem. Eng. Sci.* **1960**, *12*, 152.

(7) Hilz, E.; Vermeer, A.; Cohen Stuart, M.; Leermakers, F. A. M. Mechanism of perforation based on spreading properties of emulsified oils. *Atomization Sprays* **2012**, *22*, 1053s.

(8) Vernay, C.; Ramos, L.; Ligoure, C. Bursting of Dilute Emulsion Based Liquid Sheets Driven by a Marangoni Effect. *Phys. Rev. Lett.* **2015**, *115*, 198302−5.

(9) Vernay, C.; Ramos, L.; Ligoure, C. Free radially expanding liquid sheet in air: time and space resolved measurement of the thickness field. *J. Fluid Mech.* **2015**, *764*, 428−444.

(10) Fay, J. A. In *The spread of oil slicks on a calm sea*; Hoult, D., Ed.; Plenum Press: New York, 1969.

(11) Bergeron, V.; Langevin, D. Monolayer spreading of poly dimethylsiloxane oil on surfactant solutions. *Phys. Rev. Lett.* **1996**, *76*, 3152−3155.

(12) Dussaud, A. D.; Troian, S. M. Dynamics of spontaneous spreading with evaporation on a deep fluid layer. *Phys. Fluids* **1998**, *10*, 23−38.

(13) Harkins, W. D. A general thermodynamic theory of the spreading of liquids to form duplex films and of liquids or solids to form monolayers. *J. Chem. Phys.* **1941**, *9*, 552−568.
(14) Denkov, N. D.; Marinova, K. G.; Tcholakova, S. S. Mechanistic understanding of the modes of action of foam control agents. *Adv. Colloid Interface Sci.* **2014**, *206*, 57−67.
(15) Bergeron, V.; Fagan, M. E.; Radke, C. J. Generalized entering coefficients: a criterion for foam stability against oil in porous media. *Langmuir* **1993**, *9*, 1704−1713.
(16) Cabane, B.; Duplessix, R. Organization of surfactant micelles adsorbed on a polymer molecule in water: a neutron scattering study. *J. Phys. (Paris)* **1982**, *43*, 1529−1542.
(17) Molino, F. R.; Berret, J. F.; Porte, G.; Diat, O.; Lindner, P. Identification of flow mechanisms for a soft crystal. *Eur. Phys. J. B* **1998**, *3*, 59−72.
(18) Hayakawa, K.; Kwak, J. T. C. In *Cationic surfactants physical chemistry*; Rubingh, D. N., Holland, P. M., Eds.; Marcel Dekker Inc.: New York, 1991; p 189.
(19) Rozhkov, A.; Prunet Foch, B.; Vignes Adler, M. Dynamics of a liquid lamella resulting from the impact of a water drop on a small target. *Proc. R. Soc. London, Ser. A* **2004**, *460*, 2681−2704.
(20) Hotrum, N. E.; van Vliet, T.; Cohen Stuart, M. A.; van Aken, G. A. Monitoring Entering and Spreading of Emulsion Droplets at an Expanding Air/Water Interface: A Novel Technique. *J. Colloid Interface Sci.* **2002**, *247*, 125−131.
(21) Villermaux, E.; Bossa, B. Drop fragmentation on impact. *J. Fluid Mech.* **2011**, *668*, 412−435.
(22) Nguyen, A. V.; Evans, G. M. Stream function, flow separation and force equation for stagnation flow passing a small solid sphere touching a rising gas bubble. *J. Phys. A: Math. Gen.* **2003**, *36*, 9105−9117.
(23) Brenner, H. The Slow Motion of a Sphere Through a Viscous Fluid Towards a Plane Surface. *Chem. Eng. Sci.* **1961**, *16*, 242−251.
(24) Bonfillon, A.; Sicoli, F.; Langevin, D. Dynamic surface tension of ionic surfactant solutions. *J. Colloid Interface Sci.* **1994**, *168*, 497−504.
(25) Weinheimer, R. M.; Evans, D. F.; Cussler, E. L. Diffusion in surfactant solutions. *J. Colloid Interface Sci.* **1981**, *80*, 357−368.
(26) Matuura, R.; Kimizuka, H.; Miyamoto, S.; Shimozawa, R. The Study of the Adsorption of Detergents at a Solution Air Interface by Radiotracer Method. I. Adsorption Isotherm for the Solution of Sodium Alkyl Sulfates. *Bull. Chem. Soc. Jpn.* **1958**, *31*, 532−538.
(27) Israelachvili, J. *Intermolecular and Surface Forces*, third ed.; Academic Press, 2011.
(28) Butt, H. J.; Graf, K.; Kappl, M. *Physics and Chemistry of Interfaces*; Wiley VCH, 2003.
(29) Meunier, J. J. *J. Phys.* **1987**, *48*, 1819−1831.
(30) Denkov, N. D. Mechanisms of Foam Destruction by Oil Based Antifoams. *Langmuir* **2004**, *20*, 9463−9505.
(31) Dexter, R. W. *Pesticide formulations and application systems: 20th Volume*; Viets, A. K., Tann, R. S., Mueninghoff, J. C., Eds.; ASTM STP1400; ASTM International, **2001**; p 2710.1520/STP10432S.